Hindawi
Geofluids
Volume 2023, Article ID 6314590, 14 pages
https://doi.org/10.1155/2023/6314590

Research Article

Experimental Study on Permeability and Deformation Characteristics of Bedding Shale under Triaxial Shear-Seepage Coupling

Zhinan Lin[1], **Shihong Feng**[1], **Jiaquan Wang**[1], **Qiang Zhang**[2], **Haifeng Long**[1] and **Guangming Chen**[3]

[1]*College of Civil and Architectural Engineering, Guangxi University of Science and Technology, Liuzhou 545006, China*
[2]*China Institute of Water Resources and Hydropower Research, Beijing 100048, China*
[3]*PowerChina Kunming Engineering Corporation Limited, Yunnan 650051, China*

Correspondence should be addressed to Jiaquan Wang; wjquan1999@163.com

Received 30 June 2022; Revised 22 May 2023; Accepted 2 June 2023; Published 19 July 2023

Academic Editor: Tianshou Ma

The bedding structure of shale is generated during the deposition and formation, which results in shales with prominent anisotropic characteristics. It depends on stability, control of oil and gas storage, and deep exploitation. In addition, the mechanical and permeability parts of bedding shale are very complex when it is under deep underground space with coupled high stress and high seepage. In this study, the black bedding shale was used as the research object, and a series of triaxial shear-seepage coupling tests were carried out. Firstly, the triaxial shear stress-shear strain curves and permeability-shear stress curves of different bedding shales under other triaxial shear-seepage coupling conditions were obtained. Secondly, the failure characteristics and shear deformation characteristics of shale under the shear-seepage coupling effect were explored. The shear stress threshold and permeability evolution law at each stage of shear failure were discussed. Thirdly, the shear strength, failure mode, and mechanism parameters of the black bedding shale under different normal stress and seepage pressure were studied. Fourthly, the linear M-C criterion, Ramamurthy criterion, and Hoek-Brown criterion characterize the variation of damage strength of shale with bedding orientation under triaxial shear-seepage coupling. Those results provide an experimental basis for exploring the anisotropic mechanical characteristics and failure mechanism of bedding shale under shear-seepage coupling.

1. Introduction

In recent years, shale gas stored in shale has been a critical, unconventional, strategic supplementary energy source. Black shale is a sedimentary rock with complex compositions, and a large number of black bedding shales exist in southwest China. Due to the accumulation of the mesomineral particles during the depositional formation process, the shale has an apparent bedding structure and anisotropic mechanic characteristics [1, 2]. During the extraction of shale oil and shale gas, it is essential that keep the stability of the deep vertical and horizontal wells under the coupling conditions of high ground stress and high seepage pressure. The stability of shale in horizontal shaft wells is one of the technical bottlenecks of deep-buried shale gas development under high in situ stress and seepage pressure coupling. However, because the anisotropy of shale is complex and difficult to understand, borehole instability is often not controlled in a timely manner, resulting in frequent borehole collapse [3]. Therefore, it is of practical significance to study the anisotropic strength characteristics, behavior mechanism, and failure laws of shale under shear-seepage coupling conditions.

Some scholars have studied the anisotropic mechanical characteristics of shale with different bedding structures [4, 5]. Mokhtari and Tutunco [6] studied the anisotropic behavior of shale at different temperatures through a series of triaxial stress-seepage coupling tests. Jin et al. [7] investigated the static mechanical properties of Marcellus shale, which showed prominent anisotropic characteristics in both mechanical and

damage mechanisms. In addition, it is found that the anisotropy of bedding shale gradually decreases with the increase of confining pressure [8–10]. Cao et al. [11] studied the failure modes and fragment fractal behaviors of marine shale based on the characteristics of elastic strain energy in the failure process of shale and proposed a new scheme to evaluate the anisotropy of shale by using the relationship between fractal dimensions and elastic strain energy. Li et al. [12] established the forward modeling theory of anisotropy and proposed a quantitative evaluation method to evaluate the influence of the anisotropy properties of bedding shale on seismic wave fields. Based on an undrained multistage triaxial compression test, Piane et al. [13] studied the mechanical properties and anisotropy characteristics of wave velocity in salt-saturated shale and obtained the influence of anisotropic stresses on the anisotropy characteristics of ultrasonic wave velocity. Wang et al. [14] studied the sound velocity and acoustic emission of bedding shale. Heng et al. [15] studied the shear fracture evolution mechanism and bedding direction effect of shale with different beddings by direct shear test. Jia et al. [16] established a microscopic physical model of shale fracture slip based on shale fracture shear slip test and discussed the microscopic control mechanism of shale mineral composition on shear strength and stability evolution. Lu et al. [17] carried out direct shear tests on bedding shale and proposed a new anisotropic shear failure criterion considering the microstructure and anisotropy of shale. A large number of researchers [18–21] conducted a Brazilian splitting test on disc-shaped bedding shale samples, and the results show that when the loading direction is different from the bedding direction, there are apparent anisotropic characteristics in splitting tensile strength, brittle strength, and failure mechanism.

Besides, some scholars studied the influence of water on the anisotropic mechanical properties of shale with different bedding structures through laboratory tests and technical means. Liu and Sheng [22] conducted CT scanning observation of shale and found that the internal structure of shale became loose after hydration and expansion by water immersion, the microfractures penetrated each other, the original fractures on the bedding surface expanded, and the anisotropy coefficient increased. Teng et al. [23] analyzed the Brazilian splitting test study on many bedding shales with different water content and concluded that the shale is affected by water, which led to the decrease of tensile strength of shale. She et al. [24] evaluated the change rule of water diffusion in shale and its damage evolution law based on the test results, and the water-related damage evolution equation of shale was derived. Lou et al. [25] used RFPA2D-Flow numerical simulation software to study the failure mechanism of shale with different bedding orientations under the coupling of seepage and stress. Carey et al. [26] used a fractured core flood device and X-ray tomography combined with FDEM simulation to study the fracture permeability behavior of shale. The results show that the bedding shale perpendicular to the direct shear load develops more complex network fractures and peak permeability. Frash et al. [27] studied the apparent permeability characteristics induced by shear fractures of bedding shale under high triaxial stress and the relationship between fracture geometry and apparent permeability through shear tests. Other scholars [28–30] have studied the stability and collapse area of shale boreholes considering the mechanical properties of natural bedding geological bodies and weak structural planes, which provide guidance and recommendations for drilling techniques in permeable, brittle, and hard bedding shale. Zhang et al. [31] analyzed the influence of water activity on shale and found that the effect of anisotropy on the compressive strength of shale decreases with the increase in water content, which is the main factor controlling the mechanical behavior.

The above studies mainly focused on the boreholes stability and considered the role of water activity during the extraction of shale oil and shale gas. However, there are few studies on the deformation and stability of borehole shale in deep horizontal wells under the coupling effect of seepage pressure and high in situ stress. Due to the different bedding direction determine the anisotropy of shale permeability, cracking characteristics, and failure strength, the characteristic of bedding direction and layer bonding strength also seriously affect the oil and gas storage capacity. Moreover, the stability of anisotropic shale cavern excavation has become a key research topic today. Therefore, this paper conducted shear seepage coupling tests for shale with different bedding directions under constant normal stress loads of 10, 20, and 30 MPa and a seepage pressure of 5 MPa. The strength, deformation, failure mode, shear failure mechanism, and other anisotropic characteristics of shale under triaxial shear-seepage coupling were studied. On this basis, the variation characteristics of the shear strength of shale under the coupling effect of triaxial shear seepage were studied, and the evolution law of permeability during the progressive damage and deformation process of shale was analyzed. The mechanism of the influence of bedding planes on strength characteristics and failure mechanism was revealed.

2. Test Principle and Method

2.1. Specimen Preparation. Black shale with a prominent bedding structure is adopted as the test samples. The bedding shale sample used in the laboratory test is from the Cambrian Qingxudong Formation in Hunan Province of China. To ensure the uniformity of the shale samples, cylindrical samples with different bedding orientations were drilled from the same core by mechanical drilling, cutting, and grinding, as shown in Figure 1. The samples were uniform in appearance and flat at the ends; the error of length and diameter is less than 0.5 mm, and the parallelism of the shale sample end is within ±0.02 mm. The size of the sample is 50×90 mm ($D \times H$), and its bedding orientations are 0°, 30°, 45°, 60°, and 90°, as shown in Figure 2. The density of the sample shall be counted by weighing, and the average density is 2.57 g/cm^3. The deviation of the density of shale from the average value is less than 0.05 g/cm^3. In addition, in order to ensure that the sample is completely saturated before the test, the shale sample is dried at 105°C, vacuumized in a vacuum barrel to -0.8 Pa for 24 h, soaked in water for 48 h, and then vacuumized again for

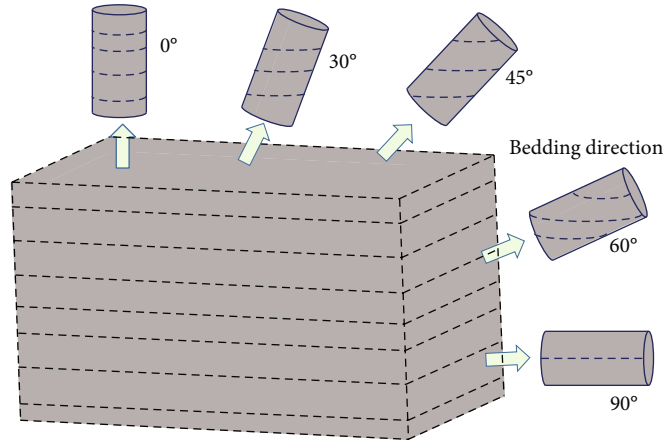

Figure 1: Schematic diagram of shale shear samples drilling.

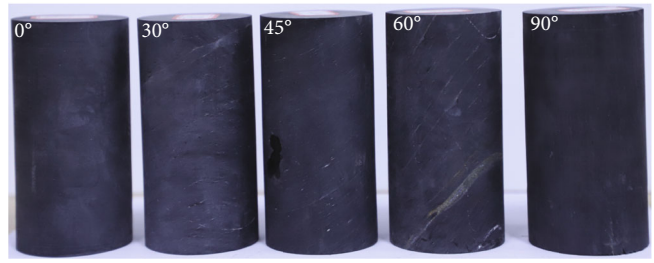

Figure 2: Shale samples with different bedding orientations.

24 h. When there is no bubble in the water, all pores in the shale sample are considered to be filled.

Shale is a kind of sedimentary rock formed by squeezing, dehydration, recrystallization, and cementation of clay with weak consolidation, but different bedding directions will be formed due to various influencing factors during sedimentation. Due to the stability problem of bedding direction in shale oil and gas mining and other engineering fields, such as mining, tunnel excavation, foundation, civil engineering, slope, nuclear waste treatment, the anisotropy of shale bedding is one of the most typical characteristics that shale-related engineering must pay attention to. Therefore, the author selected multilayered shale with bedding directions of 0°, 30°, 45°, 60°, and 90° as a sample and conducted a series of tests on the failure characteristics, shear deformation characteristics, shear strength, failure mode, and mechanism parameters of shale under constant permeability water pressure under shear seepage coupling. So the normal stress and water pressure for the tests are set to 10, 20, and 30 MPa and 5 MPa, respectively.

Figure 3 shows the mineral composition of shale based on X-ray diffraction (XRD) analysis. In general, the mineralogical composition of the bedding shale is complex, in which dolomite is the most, accounting for 45.7%. Mica is the least, accounting for 2.7%. In addition, the mineral components such as dolomite, quartz, and feldspar both have an obvious influence on the mechanical properties of shale. The uniaxial strengths of shale in different orientations are shown in Table 1.

2.2. Instrumentation. The tests were carried out in the Rock Top 50HT full-stress multifield coupling triaxial test system (Figure 4) in the laboratory of the Guangxi University of Science and Technology. The system is equipped with three independent loading systems: an axial stress loading system, normal stress loading system, and seepage stress loading system. It can apply a maximum axial shear stress of 750 MPa, maximum normal stress of 60 MPa, and maximum seepage pressure of 60 MPa. Two axial dual-channel LVDT sensors are placed on both sides of the sample. The measurement accuracy of LVDT is 0.001 mm, and the measurement range is 0~12 mm, which can accurately measure the shear displacement of the sample during the test.

2.3. Testing Principles and Procedures

2.3.1. Testing Principles. In this study, the normal stress selected for the test is 10, 20, and 30 MPa, and the seepage pressure is 5 MPa. The triaxial shear-seepage coupling test was performed on shale of different bedding orientations. Figure 5 shows the schematic diagram of the triaxial shear-seepage coupling test. As seen in Figure 5, the cushion block consists of a half-cylindrical silicone pad and cylindrical steel gaskets with permeable holes. The hardness and elastic modulus of the silicone pad are lower than that of the steel gasket. At the same axial displacement, the silicone gasket is subjected to a much smaller load than the rock. Therefore, due to the existence of the rubber pad, shear loads are formed at both ends of the rock under the action of the

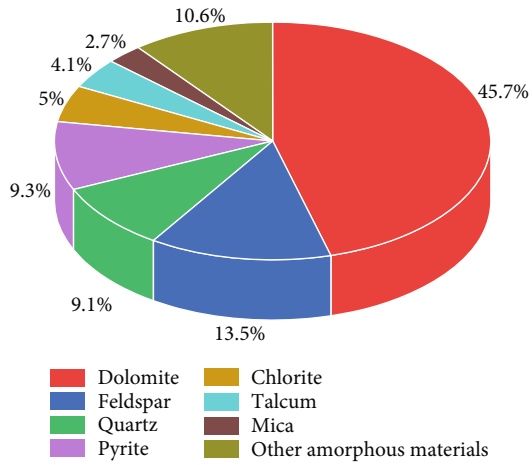

Figure 3: Mineral composition of shale with different bedding orientations.

Table 1: Uniaxial strength of shale with different bedding orientations.

Bedding orientation/°	0°	30°	45°	60°	90°
Uniaxial strength/MPa	18. 43	12. 45	6. 02	4. 58	6. 11

normal loads. By the way, the confining stress acting on the specimen is taken as the normal stress.

During the experiment, the axial force is recorded as F_0, in which the forces on the rock and silicone rubber are F' and F, respectively. The shear area of the bedding shale is recorded as S. So the shear stress τ of rock under confining pressure can be expressed as

$$\tau = \frac{F' - F}{S}, \tag{1}$$

$$F' + F = F_0, \tag{2}$$

$$\tau = \frac{F_0 - 2F}{S}, \tag{3}$$

$$F = kA\varepsilon, \tag{4}$$

where k and A are the deformation modulus and cross-sectional area of the silicone rubber, respectively.

To obtain the deformation modulus k of the silicone rubber, a uniaxial compression test is performed on a cylindrical silicone rubber with a height of 100 mm and a diameter of 50 mm. The stress-strain curve of the silicone rubber was obtained by testing, as shown in Figure 6.

2.3.2. Testing Procedures. Firstly, the bedding shale sample, the half-cylindrical silicone pad, and steel gasket are tightly wrapped in a heat-shrinkable sleeve and placed in a pressure chamber. Two LVDT displacement sensors are connected.

Secondly, when the loading rate is 10 bar/min, the normal stress was loaded from 0 MPa to the target value and stabilized for 30 min.

Thirdly, the seepage pressure at the outlet end is equal to the atmospheric pressure. The seepage pressure at the inlet end was loaded from 0 MPa to the target value at the rate of 15 bar/min and stabilized for 30 min, so that stable seepage was formed inside the sample. Moreover, the seepage pressure remains constant during the test.

Fourthly, the shear stress was loaded at a displacement loading rate of 0.02 mm/min. When the shear stress reaches the maximum value, the ductile joint is formed inside the sample, and finally, the test is completed.

During the triaxial shear-seepage coupling test, the test data were recorded every 5 s. For high-density rock materials and permeability coefficient $k \geq 10^{-7}\ \mu m^2$, the steady-state method should be used to measure permeability [32]. Due to the low porosity of shale samples, the steady-state method is used to measure permeability during the test. The permeability of the sample is calculated according to Equation (5) as follows:

$$k_i = \frac{\mu L(Q_{i+1} - Q_i)}{A\Delta P\Delta t}, \tag{5}$$

where μ is the dynamic viscosity coefficient of water, which is 1.005×10^{-3} pa. s at room temperature, L is the height of the sample (m), A is the cross-sectional area of the rock sample, Q_i and Q_{i+1} are the seepage flow at the i-th and $i+1$ -th recording points, respectively; Δt is the time interval between the i and the $i+1$ recording point, and ΔP is the seepage pressure difference between both ends of the sample within the time Δt.

3. Experimental Results and Discussions

3.1. Shear Stress-Shear Strain Curve. The macroscopic failure and deformation process of bedding shale under loading is the process of closuring, initiation, expansion, and penetration of microscopic cracks. Figures 7 and 8 show the shear stress-shear strain curves of shale with different bedding orientations in the triaxial shear-seepage coupling test. According to the compression-shear deformation and fracture development of bedding shale under hydraulic coupling, this paper introduces the concept of shear stress threshold. It analyzes the change law of the triaxial shear stress threshold of shale, which is essential for the stability monitoring of rock engineering.

The shear stress thresholds for each stage of shear deformation are now marked as points A, B, C, D, and E, respectively. The shear stress-shear strain curve of bedding shale can be divided into the prepeak area and postpeak area, as shown in Figure 7. The prepeak area can be divided into four stages based on the fracture development characteristics and the shear stress deformation thresholds during the failure process of bedding shale, the prepeak area is divided into four stages. They are the initial microcrack and void compaction stage (OA), crack initiation stage (AB), shear crack initiation and development stage (BC), and crack extension and damage stage under compression shear action (CD), respectively. For those four stages, the corresponding thresholds are microcrack closure shear stress (τ_{cc}), crack initiation

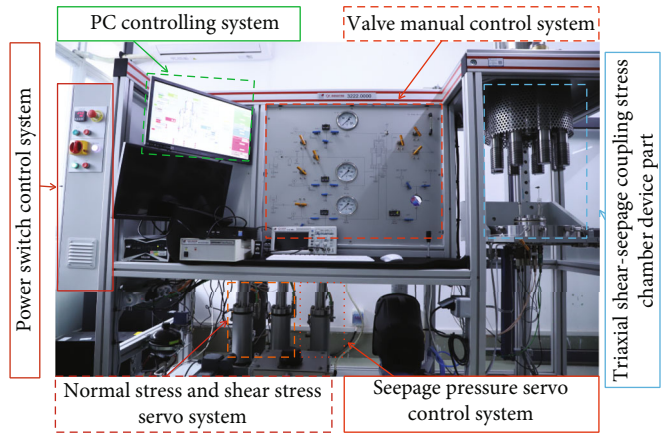

Figure 4: Rock Top 50HT full stress multifield coupled triaxial test system.

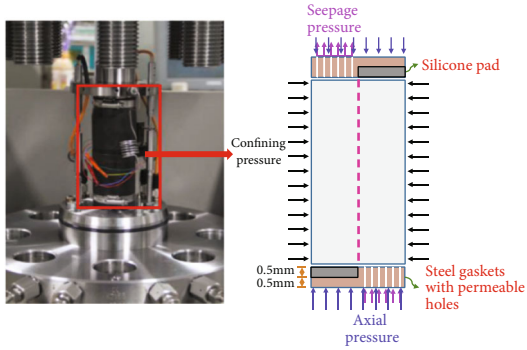

Figure 5: Schematic diagram of the triaxial shear-permeability coupling test.

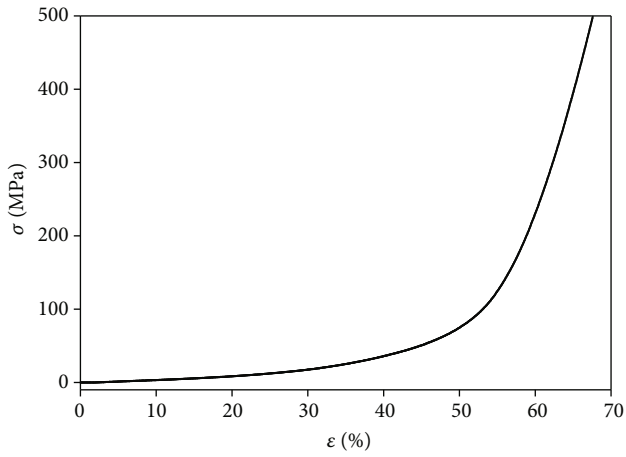

Figure 6: Stress-strain curve test of silicone rubber.

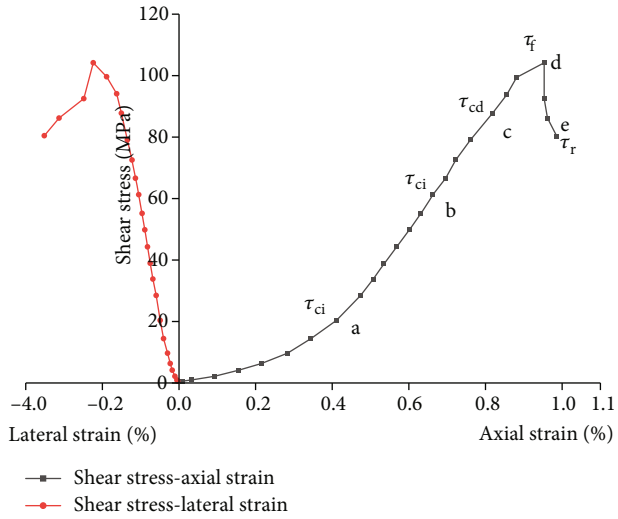

Figure 7: Five stages of shear damage under triaxial shear-seepage coupling test (normal stress = 10 MPa, seepage pressure = 5 MPa).

shear stress (τ_{ci}), crack damage shear stress (τ_{cd}), and peak shear strength (τ_f), respectively. The postpeak area is the postpeak shear failure stage (DE), and the corresponding shear stress threshold is the residual shear strength (τ_r). The characteristics for those stages are as follows:

In the first stage (initial microcrack and void compaction stage OA), the triaxial shear-seepage coupling initiation stage, the shear stress-shear strain curves of bedding shales show nonlinear characteristics. It is mainly due to the bedding plane, primary cracks, many voids, and micropores of bedding shales gradually compaction under the combined action of normal stress, shear stress, and seepage stress, and the volume is gradually squeezed and shrunk. At the initial stage, the shear stress-shear strain curve is concave, but the microcrack closure shear stress is different from judging and calculating according to the shear stress-shear strain curve. In this study, the method based on axial shear strain difference was adopted to determine the closed shear stress of microcracks [33]. Due to the rock matrix is contact with each other, the axial shear stress reaches the microcrack closure shear stress (τ_{cc}), and the original crack and voids have been completely closed.

In the second stage (crack initiation, linear elastic stage AB), the axial shear stress-shear strain curve of bedding shale is approximately linear; in other words, the axial shear stress of bedding shale increases linearly with the increase of axial shear strain. The ratio of shear stress increment to shear strain increment in this stage is the shear elastic

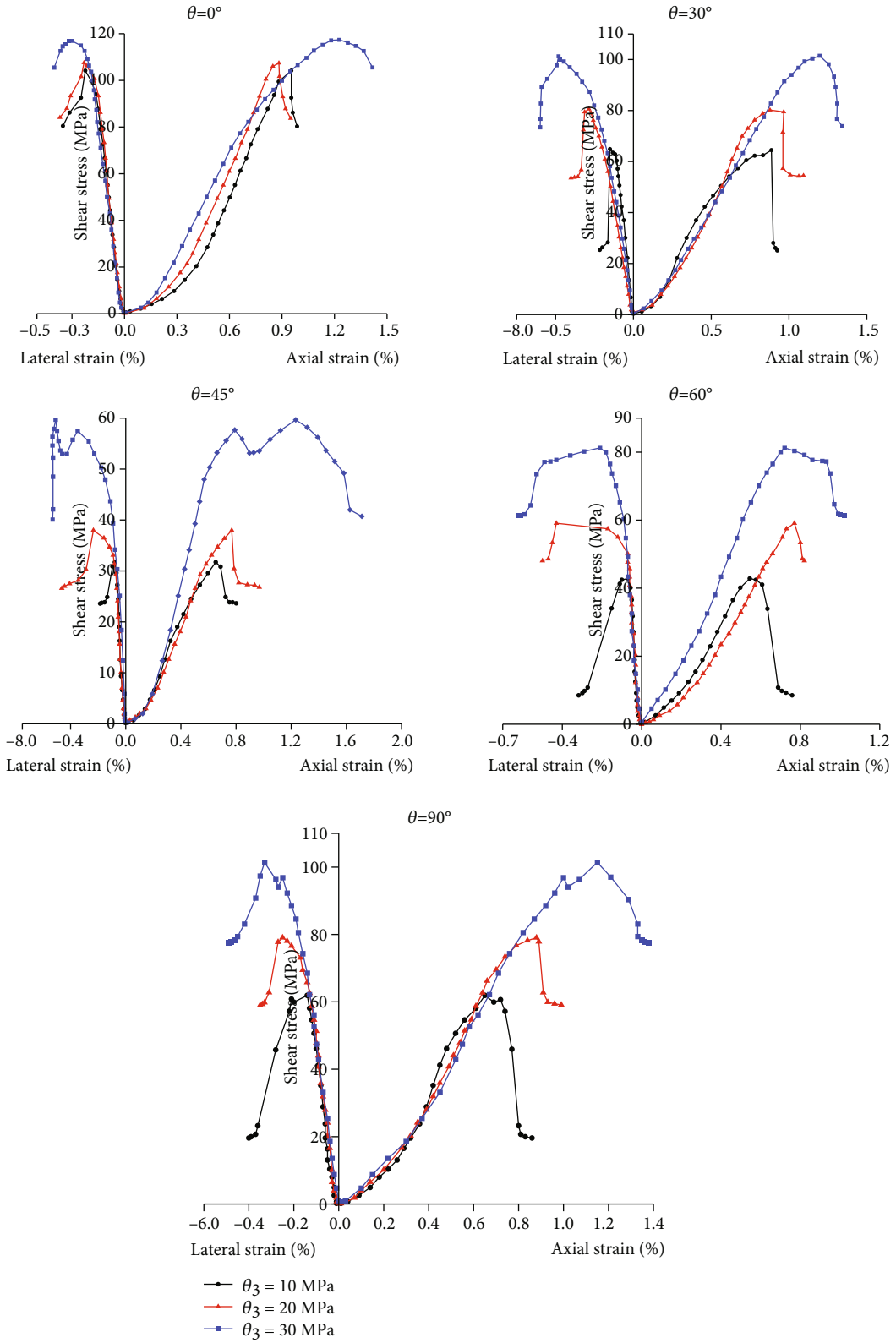

Figure 8: Shear stress-shear strain curves of shales with different bedding orientations (seepage pressure = 5 MPa).

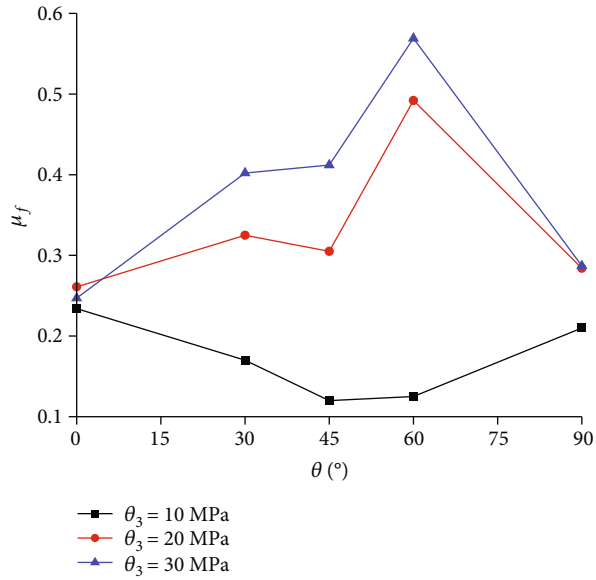

Figure 9: The relation curve between generalized Poisson's ratio and bedding orientation under different normal stresses (seepage pressure = 5 MPa).

deformation modulus. At this time, the volumetric strain of bedding shale is approximately equal to the elastic volumetric strain. The internal primary fractures and voids continue to be compacted, and the volumetric compression rate decreases gradually.

In the third stage (crack initiation and development stage BC), the shear stress-shear strain curve of bedding shale exhibits nonlinear characteristics. This stage is the initial developmental stage of plastic deformation. When the axial shear stress of bedding shale exceeds the initial shear stress of crack (τ_{ci}), the primary cracks and pores are no longer compacted, and the internal cracks begin to initiate and expand slowly and stably, but to a certain extent, no macroscopic cracks were formed.

In the fourth stage (crack damage propagation stage CD), when the shear stress exceeds the crack damage shear stress (τ_{cd}), the shear stress-shear strain curve of bedding shale still shows nonlinear deformation characteristics, but the slope of the curve decreases gradually. This is due to the unstable propagation of the newly developed cracks after the shear stress reaches the damage dilatancy shear stress, and the new shear prominent cracks are initially formed. With the continuous development of shear stress, the volumetric strain of bedding shale slowly transforms from compression to expansion. The permeability of bedding shale at this stage will increase rapidly with the generation of prominent shear cracks.

In the fifth stage (postpeak failure stage DE), with the increase of shear stress under external load, the primary shear fracture continues to expand unstably, then the bedding shale would be further damaged. Brittle failure of bedding shale is formed under low normal pressure, and tensile failure is formed under high normal pressure.

Figure 8 shows the shear stress-radial strain curve of bedding shale in the triaxial shear-seepage coupling test. During the triaxial shear-permeability coupling test, the radial deformation of bedded shale experienced three typical stages, including slow deformation, linear deformation, and gradual expansion deformation. The maximum radial strain of bedding shale under different normal stresses is less than 1%. When the shale fails, the absolute value of the ratio of its radial shear strain to axial shear strain is defined as the generalized Poisson's ratio, which can reflect the radial deformation characteristics of shale in the triaxial shear-seepage coupling test. The calculation in Equation (6) is as follows:

$$\mu_f = \left|\frac{\varepsilon_{3f}}{\varepsilon_{1f}}\right|, \tag{6}$$

where the parameters ε_{1f} and ε_{3f} are the axial shear strain and radial shear strain when shale fails during the triaxial shear-seepage coupling test.

When the seepage pressure is 5 MPa, the relationship between the generalized Poisson's ratio and the bedding orientation of bedding shale under different constant normal stresses is shown in Figure 9. With the increase of the normal stress, the generalized Poisson's ratio μ_f of bedding shale increases, and the growth of the bedding orientation of 60° and 0° is the maximum and minimum, respectively. The generalized Poisson's ratio μ_f ranges from 0.125 to 0.569 when the normal stress increases from 10 MPa to 30 MPa. In addition, the radial strain deformation of rock has noticeable characteristic changes under the triaxial stress-seepage coupling conditions [34–36]. The radial strain of rock under the triaxial shear-seepage coupling test is much smaller than that under the triaxial stress-seepage test. Compared with the boundary condition of constant normal stiffness, the radial variation amplitude of the triaxial shear test under constant normal stress is more significant [37].

3.2. Shear Failure Characteristics of Shale. The failure characteristics of bedding shale under shear-seepage coupling are shown in Figure 10. The white dotted line and thickness in Figure 10 represent the location and size of the fracture surface, respectively. Due to the restraint of normal stress, the weakening of seepage pressure, and the attenuation effect of the bedding plane, the failure characteristics of bedding shale become more complex. Previous studies have shown that shale is fractured into small fragments under uniaxial compression [38, 39]. Under triaxial compression, the main failure modes of shale include axial splitting failure, single shear failure, conjugate shear failure, and ductile deformation failure. In this study, the failure mode of shale under triaxial shear-seepage coupling conditions is mainly as follows:

(1) Shear failure along the shear plane. When the bedding orientation is 90°, as shown in Figure 10, in the triaxial shear-seepage coupling condition, the shear failure surface is a top-bottom shear surface with small cracks on both sides of the fracture

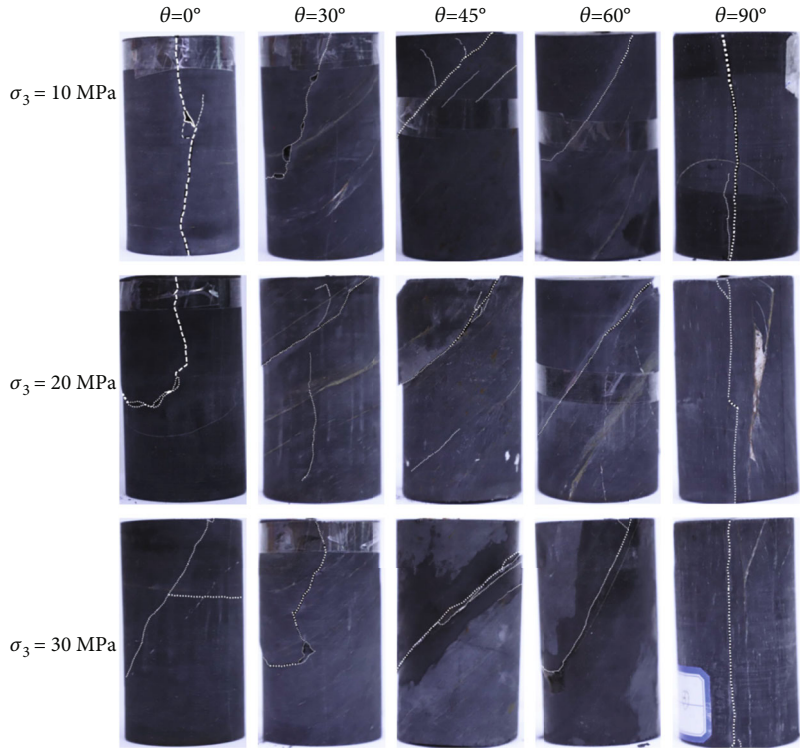

Figure 10: Failure mode of bedding shales with different bedding orientations.

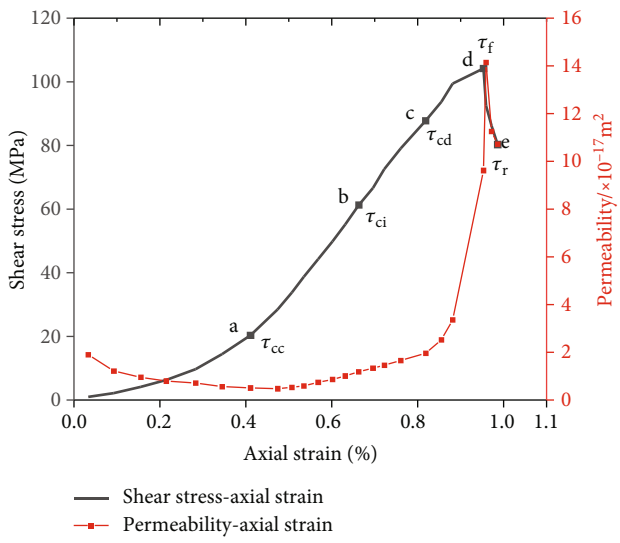

Figure 11: Shear stress-permeability-axial strain curf of bedding shale under triaxial shear-seepage coupling condition ($\theta = 0\circ$, σ_3 = 10 MPa).

surface, and there are small cracks on both sides of the fracture surface

(2) Sliding failure along the bedding plane. As shown in Figure 10, these failures mainly occur at the bedding orientation θ of 45° and 60°, sliding along the bedding structural plane before the shear zone is formed, and the failure cracks of the bedding shale extend along the bedding plane. It is due to the shear strength of the bedding plane being less than the tangential component of the shear stress on the bedding plane

(3) Shear-sliding combination failure. This failure mode mainly occurs in shale with a bedding orientation of 0°-30°. As shown in Figure 10, the failure samples contain axial shear damage cracks and damage cracks along the sliding surface

(4) Transverse shear failure. When the bedding orientation is 0° and the normal stress is 30 MPa, the failure samples contain transverse cracks forming conjugate shear cracks

3.3. Permeability Characteristics of Shales. The permeability of bedding shale under the triaxial shear-seepage coupling test is calculated by Equation (5). Figure 11 shows the permeability-shear stress curves of bedding shale under different normal stresses when the seepage pressure is 5 MPa. Due to the limited space, this paper only takes the shear stress-shear strain-permeability curve of shale with bedding orientation of 0° under normal stress of 10 MPa as an example. It can be seen from Figure 11 that with the increase of axial shear strain, the permeability first decreases slowly, then increases gradually, and then increases sharply until reaching the maximum value. When the axial shear strain increases continuously, the permeability decreases rapidly and finally tends to be stable. In addition, with the gradual development of shear strain, the trend of the permeability-shear strain curve lags behind the movement of triaxial shear stress-shear strain curve. To be consistent with the shear

stress segmentation of bedding shale during the triaxial shear-seepage coupling test in the previous paper, the shear stress-shear strain curve, and permeability curve are divided into five stages: OA, AB, BC, CD, and DE, as shown in Figure 11.

According to the triaxial shear stress-permeability-shear strain curve in Figure 11, it can be known that in the early shear deformation stage (OB stage) of bedding shale under the triaxial shear–seepage coupling, when the shear stress-shear strain curve is in the nonlinear deformation OA section, the permeability of the bedding shale decreases gradually. Because at the beginning of shear stress loading, the fractures inside the shale are progressively closed, and the seepage channels inside the shale are continuously compacted, leading to the gradual reduction of the permeability of the bedding shale.

With the increase of axial shear stress, the permeability of elastic deformation AB shale increases slowly. When the shear stress exceeds τ_{ci} (BC stage), the internal fractures of bedding shale will gradually initiate and connect, resulting in the gradual increase of permeability of the bedding shale.

When the shear stress increases gradually and reaches the τ_{cd} (CD stage), under the condition of triaxial shear-seepage coupling, the main fractures will gradually form inside the shale, which is the main seepage channel. In addition, with the increase of newly generated fractures, the seepage channels inside the shale increase, so its permeability increases rapidly.

When the shear stress exceeds τ_f, the shale has been destroyed, primary fractures (DE stage) have been formed inside the shale, and the permeability of the shale gradually reaches the maximum value. The primary shear fracture is the dominant factor controlling the permeability of shale. At the later stage of axial shear stress loading, the permeability of shale gradually decreases and tends to be stable. After the formation of shear failure, with the further increase of shear displacement, the shear stress of the sample gradually decreases, the permeability gradually increases and reaches the maximum value, and the peak permeability obviously lags behind the peak shear strength. When the shear displacement continues to increase, the shear fracture surface slips relatively, and under the action of constant normal stress, the fracture surfaces on both sides are closed again, and the shear wear particles are filled between the fracture surfaces, so that the permeability will decrease sharply, which is similar to the permeability evolution law of rock in the process of hydrostatic pressure and triaxial compression deformation by Xiao et al. [33] and Yu et al. [34].

In engineering practice, the evolution law of permeability in the progressive failure process before rock failure is the key issue that engineers are concerned about. Therefore, this paper further studies the permeability evolution characteristics of bedding shale under the increase of shear stress. Figure 12 shows the permeability-shear stress curves of shale under the triaxial shear-seepage coupling conditions. At the initial stage of shear stress growth, the permeability of shale decreases with the increase of shear stress, which is related to the compaction of the internal pores and fractures in bedding shale. With the further expansion of shear stress, the permeability of bedding shale gradually changes from a decreasing state to an increasing state, which is due to the generation of new fractures inside the bedding shale, resulting in the rise of seepage channels. In summary, under the triaxial shear-seepage coupling condition, the permeability corresponding to the peak strength decreases, and the permeability amplitude gradually decreases with the increase of the normal stress.

3.4. Failure Mechanism of Shale under Shear-Seepage Coupling Condition

3.4.1. Shear Strength Characteristics of Shales with Different Bedding Orientations. In the triaxial shear-seepage coupling test, the shear stress characteristic values of shale with different bedding orientations can directly reflect the deformation characteristics of corresponding stages. The crack closure shear stress τ_{cc} is defined as the boundary shear stress when the bedding shale changes from the initial compaction stage to the linear elastic deformation stage; the crack initiation shear stress τ_{ci} is the boundary shear stress when the bedding shale ends the elastic deformation stage and the plastic deformation stage begins. The crack damage shear stress τ_{cd} is the critical shear stress when the bedding shale changes from volume compression deformation to volume expansion; the peak shear stress τ_f is the maximum shear stress of shale with different bedding orientations under the triaxial shear-seepage coupling test.

Table 2 is the summary table of the characteristic shear stress of bedding shale with different bedding orientations at each corresponding stage during the triaxial shear-seepage coupling test. Under the same normal stress, crack closure shear stress τ_{cc}, crack initiation shear stress τ_{ci}, crack dilatancy shear stress τ_{cd}, and peak shear stress τ_f, all show nonlinear characteristics with the increase of the bedding orientation of shale. The ratio of crack closure shear stress to peak shear stress τ_{cc}/τ_f is between 0.15 and 0.25; the ratio of crack initiation shear stress to peak shear stress τ_{ci}/τ_f is between 0.42 and 0.61; the ratio of crack damage shear stress to peak shear stress τ_{cd}/τ_f is between 0.72 and 0.86. The main reason why the characteristic stress exhibits large anisotropy is that shale is mainly composed of the primary bedding structure plane.

Various minerals in the same interlayer are closely and regularly arranged, and their mechanical parameters are high; their mechanical parameters are low when the primary bedding plane is a weak structural plane. The failure plane of shale with a bedding orientation of 0° is perpendicular to the bedding structural plane under triaxial shear-seepage coupling. Its shear failure strength is significantly higher than that of shale with other bedding orientations. When the bedding orientations are 30, 45, 60, and 90°, the characteristics of shear stress of shale are affected not only by the normal stress, axial shear stress, and seepage pressure during the triaxial shear-seepage coupling test but also affected by the bedding orientations of shale. In summary, the shear sliding of each bedding plane induces the expansion of internal

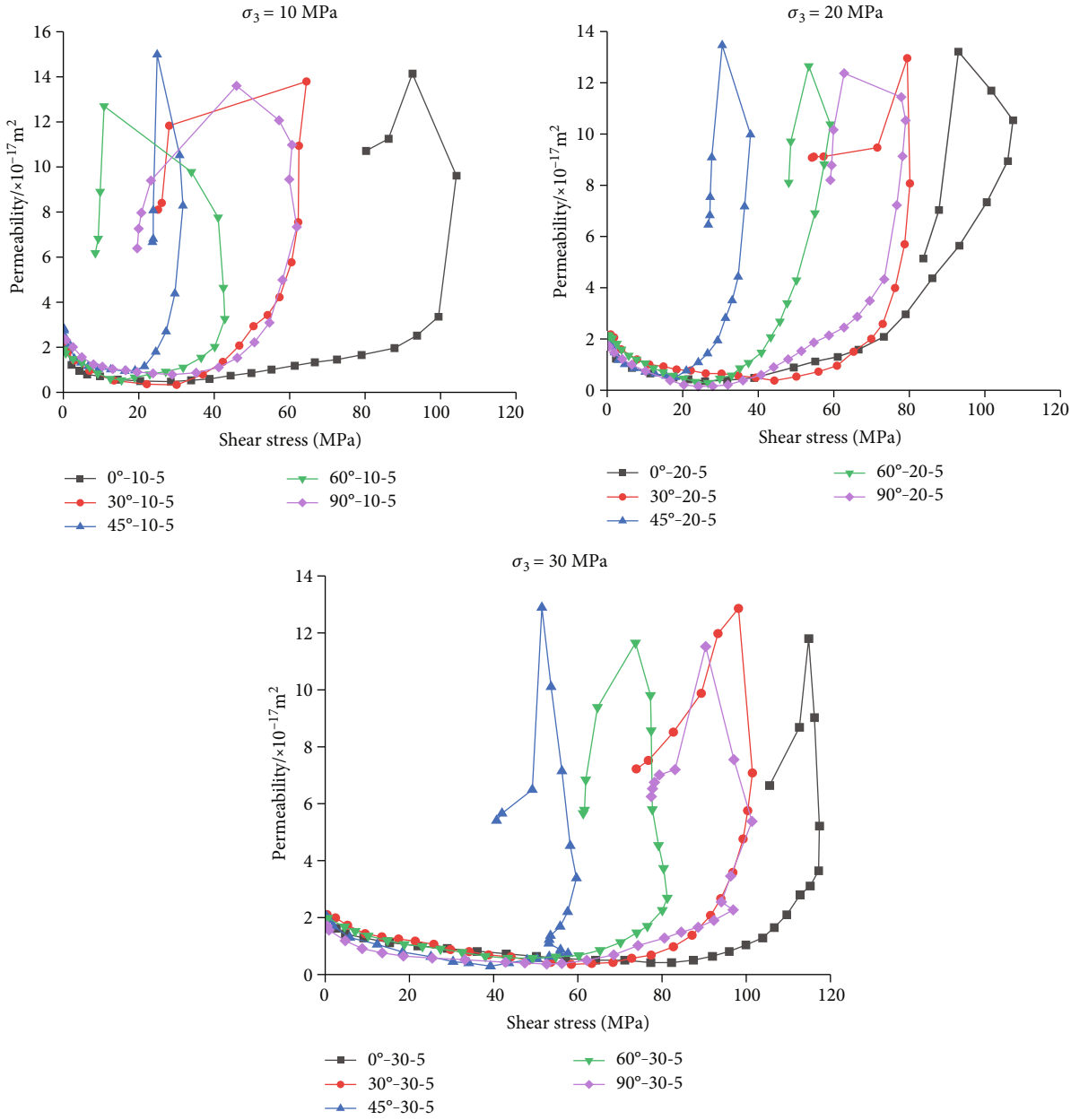

Figure 12: The permeability-shear stress curves of bedding shale under shear-seepage condition.

cracks and pores, resulting in the relative reduction of the shear stress characteristic value and showing prominent anisotropic characteristics.

3.4.2. Analysis of Shear Strength Parameters. Triaxial shear-seepage coupling tests were carried out on the bedding shale with different bedding orientations. Figure 13 shows the shear strength of shale with different bedding orientations obtained under the normal stress of 10, 20, and 30 MPa.

As shown in Figure 13, with the increase of bedding orientation, the shear strength of shale shows a trend of first decreasing and then increasing, which is positively correlated with the normal stress. Under the normal stress of 10 MPa, the shear strength of the shale with a bedding orientation of 0° is 103.791 MPa. With the increase of the bedding orientation, the shear strength of the shale is distributed in a "shoulder" shape. Based on Mohr-Coulomb theory, the failure mode of shale is mainly a shear failure, which is closely related to normal stress and shear stress, and the shear strength of shale is determined by the cohesion and internal friction angle. The expression of Mohr-Coulomb theory is as follows:

$$\tau = c + \sigma \tan \varphi, \tag{7}$$

where the parameters c and τ are the cohesion and internal friction angle, respectively.

According to the above formula, the cohesive force and internal friction angle under different bedding orientations can be obtained, as shown in Figure 14.

Table 2: The shear stress characteristic values of shale with different bedding orientations under triaxial shear - seepage coupling test.

No.	σ_3/MPa	θ/°	τ_{cc}/MPa	τ_{ci}/MPa	τ_{cd}/MPa	τ_f/MPa	τ_{cc}/τ_f	τ_{ci}/τ_f	τ_{cd}/τ_f
Y-01		0	16.67	61.47	82.30	104.18	0.16	0.59	0.79
Y-02		30	9.67	36.74	50.92	64.45	0.15	0.57	0.79
Y-03	10	45	5.39	16.17	22.83	31.71	0.17	0.51	0.72
Y-04		60	7.71	22.70	31.69	42.83	0.18	0.53	0.74
Y-05		90	13.00	26.00	45.81	61.90	0.21	0.42	0.74
Y-06		0	21.49	65.53	85.94	107.43	0.20	0.61	0.80
Y-07		30	14.43	44.09	68.95	80.17	0.18	0.55	0.86
Y-08	20	45	6.83	19.36	30.37	37.96	0.18	0.51	0.80
Y-09		60	10.05	31.32	49.04	59.09	0.17	0.53	0.83
Y-10		90	15.01	41.09	61.64	79.02	0.19	0.52	0.78
Y-11		0	25.82	71.60	100.95	117.38	0.22	0.61	0.86
Y-12		30	17.25	53.78	82.19	101.47	0.17	0.53	0.81
Y-13	30	45	10.14	32.82	47.74	59.67	0.17	0.55	0.80
Y-14		60	16.25	40.64	60.14	81.27	0.20	0.50	0.74
Y-15		90	20.28	47.65	78.06	101.38	0.20	0.47	0.77

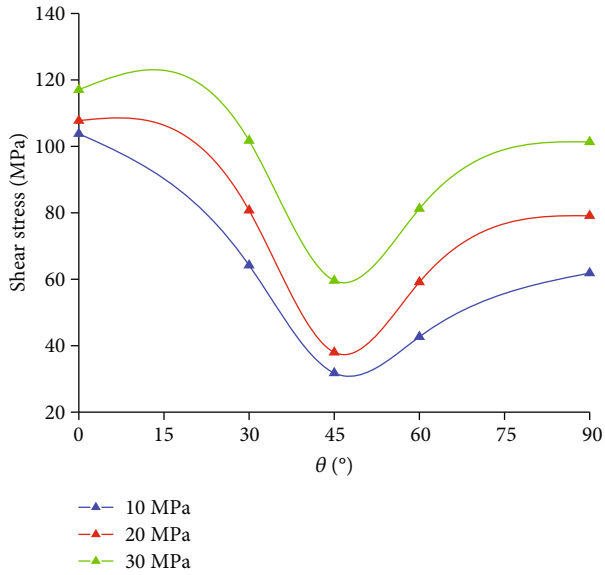

Figure 13: Shear strength of different bedding shales under different normal stresses.

It can be seen from Figure 14 that when the bedding orientation increases, the value of cohesion presents a "U" curve, which indicates that the cohesion of bedding shale has anisotropic characteristics under the triaxial shear-seepage coupling condition. The internal friction angle (φ) does not show a specific pattern as the bedding orientation is increases. When the bedding orientation is 0°, it is difficult for the shear fractures inside the shale to cross the bedding surface after failure because the bedding surface inhibits the expansion of the primary shear fractures; thus, it has considerable cohesion and slight internal friction angle. When the bedding orientation increases gradually, the newly formed fractures will expand and develop along the bedding plane, resulting in lower cohesion. In addition, when the bedding orientation is 45°, the cohesion of shale is the minimum.

Strength parameters are essential for evaluating the mechanical properties of shales with different bedding orientations. The generalized Hoek-Brown criterion [40] based on the Griffith crack theory is an empirical strength criterion. It has been widely used to describe the nonlinear behavior of shear strength. The criterion is as follows:

$$\sigma_1 = \sigma_3 + \sqrt{m\sigma_u\sigma_3 + s\sigma_u^2}, \tag{8}$$

where m and s are the two strength parameters in the Hoek-Brown criterion, and σ_u is the uniaxial compressive strength of intact bedding shale. Parameters m and s are constants for the entire rock. When the parameter m is larger, the stone is more substantial. The parameter s reflects the incompleteness degree of the rock, the value ranging from 0 to 1; when the parameter s is close to 1, the stone is intact.

In general, for significant rocks, the parameters m and s are constant, while for anisotropic rocks, the parameters m and s are inconsistent. Therefore, through a series of triaxial shear-seepage coupling tests on shales with different bedding directions, the strength parameters m and s of shales are determined. According to the m and s values of anisotropic rocks, the failure strength of different bedding shales can be predicted under triaxial shear-seepage coupling. In this study, the shale samples from each bedding direction were considered intact; therefore, the parameter s of shale was 1. The triaxial shear-seepage coupling test data is substituted into Equation (8) to obtain the parameter m of the specimen at each bedding orientation.

Ramamurthy and Arora [41] proposed the following expression based on the complete nonlinear yield strength

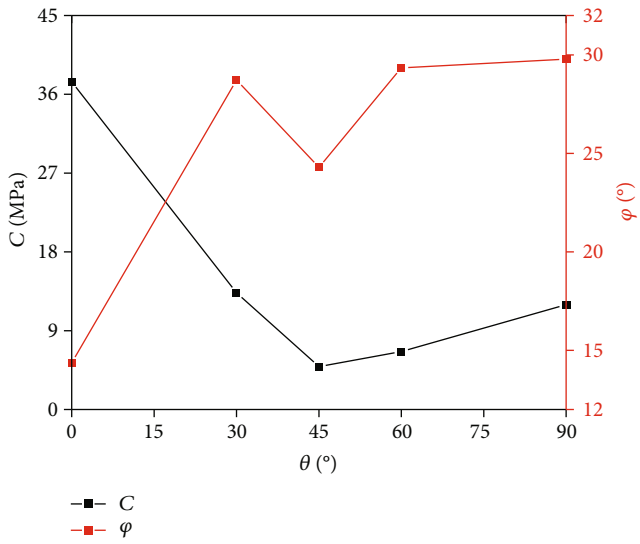

Figure 14: Variation curve of c and φ with the shale bedding orientation using Mohr-Coulomb criterion.

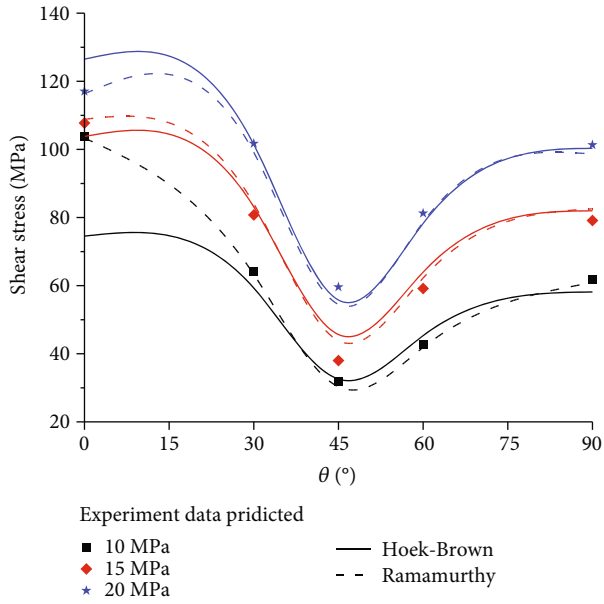

Figure 15: Curves of test and strength prediction values versus bedding orientation under different normal stresses.

criterion for anisotropic rocks:

$$\frac{\sigma_1 - \sigma_3}{\sigma_3} = B_i \left(\frac{\sigma_c}{\sigma_3}\right)^{\alpha_i}, \tag{9}$$

where α_i and β_i are considered strength parameters.

According to Ramamurthy (1994), for rock masses, even intact anisotropic rocks, the values of the parameters α_i and β_i are not constant, which change with their uniaxial strength, loading direction, and the bedding orientation. Figure 15 shows the predicted values from two different predicted empirical equations and test data under the triaxial shear-seepage coupling condition.

$$\frac{\alpha_j}{\alpha_{90}} = \left(\frac{\sigma_{cj}}{\sigma_{c90}}\right)^{1-\alpha_{90}}, \tag{10}$$

$$\frac{\beta_j}{\beta_{90}} = \left(\frac{\sigma_{90}}{\sigma_j}\right)^{0.5}. \tag{11}$$

According to the triaxial shear test data in Figure 15 and the prediction results of the Ramamurthy criterion and Hoek-Brown criterion, the consistency is very high. Figure 15 clearly reflects that the Ramamurthy criterion and the Hoek-Brown criterion can predict the experimental results under the triaxial shear-seepage coupling condition.

4. Conclusion

Considering the influence of high normal stress and seepage pressure on the shear strength and permeability characteristics of shale, this paper conducts a series of shear-seepage coupling tests on bedding shales with different bedding orientations under triaxial shear-seepage coupling conditions. The main conclusions are as follows:

(1) In the triaxial shear-seepage coupling test, when the normal stress is the same, the shear stress characteristic value and shear stress characteristic ratio of shales with different bedding orientations show a nonlinear growth trend with the increase of bedding orientation. When the bedding orientation is 0°, the shear strength is the maximum, while it is the minimum when the bedding orientation is 45°

(2) During the triaxial shear-seepage coupling test, the permeability of shale with different bedding orientations decreases first and then increases until it reaches the maximum value. When the permeability reaches the peak, it decreases rapidly and tends to be stable finally. The peak permeability lags significantly behind the peak of shear stress. In addition, the ratio of axial strain to radial strain is always much less than 1

(3) Due to the restraint of normal stress, the weakening of seepage pressure, and the attenuation effect of the bedding plane, the failure characteristics of bedding shale become more complex. It can be summarized into four typical failure modes: the shear failure along the shear plane, the sliding failure along the bedding plane, the shear-sliding combination failure, and the lateral shear failure. It can conclude that the shear failure of shale under the triaxial shear-seepage coupling condition is relatively complex

(4) With the increase of bedding direction, the shear peak strength shows a "shoulder" curve. The linear Mohr-Coulomb criterion, Ramamurthy criterion, and Hoek-Brown criterion are used to describe the failure strength of shale with different bedding orientations under triaxial shear-seepage coupling conditions. According to the relevant results, the three criteria can reasonably predict the test data

In this paper, only the triaxial shear-seepage coupling test of shale from the Cambrian Qingxudong Formation in Hunan Province of China is carried out, and the shear damage mechanism and permeability characteristics of bedding shale are analyzed in detail, which provides a new idea for studying the mechanical properties and failure modes of shale. However, the relationship between microdamage and macropermeability characteristics of bedding shale has not been established by means of micromeasurement techniques. In the future research, the microdamage mechanism of bedding shale with different bedding orientations will be further studied by confining pressure, seepage water pressure, and other factors.

Data Availability

The data used to support the findings of this study are included within the article.

Conflicts of Interest

The authors declare that there is no conflict of interest regarding the publication of this paper.

Acknowledgments

This study was funded by the Natural Science Foundation in Guangxi Province of China (No. 2021GXNSFBA196043 and 2022GXNSFDA035081), the Guangxi University Young and Middle-aged Teachers' Basic Scientific Research Ability Improvement Project (No. 2020KY08023), the Natural Science Foundation of China-Yalong River Joint Fund (No. U1965204), the Doctoral Foundation of Guangxi University of Science and Technology (No. 03200009), and the National Science Foundation of China (No. 41962017).

References

[1] X. W. Liu, Z. Q. Guo, C. Liu, and Y. W. Liu, "Anisotropy rock physics model for the Longmaxi shale gas reservoir, Sichuan Basin, China," *Applied Geophysics*, vol. 14, no. 1, pp. 21–30, 2017.

[2] H. Sone and M. D. Zoback, "Mechanical properties of shale-gas reservoir rocks - part 1: static and dynamic elastic properties and anisotropy," *Geophysics*, vol. 78, no. 5, pp. D381–D392, 2013.

[3] T. Vanorio, T. Mukerji, and G. Mavko, "Emerging methodologies to characterize the rock physics properties of organic-rich shales," *The Leading Edge*, vol. 27, no. 6, pp. 780–787, 2008.

[4] E. Fjær and O. M. Nes, "The impact of heterogeneity on the anisotropic strength of an outcrop shale," *Rock Mechanics and Rock Engineering*, vol. 47, no. 5, pp. 1603–1611, 2014.

[5] S. Heng, X. Z. Li, X. Liu, and Y. Chen, "Experimental study on the mechanical properties of bedding planes in shale," *Journal of Natural Gas Science and Engineering*, vol. 76, article 10361, 2020.

[6] M. Mokhtari and A. N. Tutuncu, "Impact of laminations and natural fractures on rock failure in Brazilian experiments: a case study on Green River and Niobrara formations," *Journal of Natural Gas Science and Engineering*, vol. 36, pp. 79–86, 2016.

[7] Z. F. Jin, W. X. Li, C. R. Jin, J. Hambleton, and G. Cusatis, "Anisotropic elastic, strength, and fracture properties of Marcellus shale," *International Journal of Rock Mechanics and Mining Sciences*, vol. 109, pp. 124–137, 2018.

[8] T. Y. Chen, X. T. Feng, X. W. Zhang, W. D. Cao, and C. J. Fu, "Experimental study on mechanical and anisotropic properties of black shale," *Chinese Journal of Rock Mechanics and Engineering*, vol. 33, no. 9, pp. 1772–1779, 2014.

[9] J. W. Cho, H. Kim, S. Jeon, and K. B. Min, "Deformation and strength anisotropy of Asan gneiss, Boryeong shale, and Yeoncheon schist," *International Journal of Rock Mechanics and Mining Sciences*, vol. 50, pp. 158–169, 2012.

[10] Q. Gao, J. L. Tao, J. Y. Hu, and X. B. Yu, "Laboratory study on the mechanical behaviors of an anisotropic shale rock," *Journal of Rock Mechanics and Geotechnical Engineering*, vol. 7, no. 2, pp. 213–219, 2015.

[11] H. Cao, Q. Gao, G. Q. Ye, H. L. Zhu, and P. H. Sun, "Experimental investigation on anisotropic characteristics of marine shale in Northwestern Hunan, China," *Journal of Natural Gas Science and Engineering*, vol. 81, article 103421, 2020.

[12] H. Li, X. W. Liu, X. Chang, R. Y. Wu, and J. Liu, "Impact of shale anisotropy on seismic wavefield," *Energies*, vol. 12, no. 23, p. 4412, 2019.

[13] C. D. Piane, D. N. Dewhurst, A. F. Siggins, and M. D. Raven, "Stress-induced anisotropy in brine saturated shale," *Geophysical Journal International*, vol. 184, no. 2, pp. 897–906, 2011.

[14] Y. Wang, H. Li, A. Mitra, D. H. Han, and T. Long, "Anisotropic strength and failure behaviors of transversely isotropic shales: an experimental investigation," *Interpretation*, vol. 8, no. 3, article SL59, 2020.

[15] S. Heng, X. Z. Li, X. Liu, and X. D. Zhang, "Study on the propagation mechanisms of shale fractures under direct shear conditions," *Chinese Journal of Rock Mechanics and Engineering*, vol. 38, no. 12, pp. 2438–2450, 2019.

[16] Y. Z. Jia, Z. H. Lu, J. R. Tang, D. H. Li, and P. He, "Friction stability and permeability response of shale fractures during shear slip," *Journal of China Coal Society*, vol. 46, no. 9, pp. 2923–2932, 2021.

[17] H. J. Lu, H. P. Xie, Y. Luo et al., "Failure characterization of Longmaxi shale under direct shear mode loadings," *International Journal of Rock Mechanics and Mining Sciences*, vol. 148, article 104936, 2021.

[18] P. Hou, F. Gao, Y. G. Yang et al., "Effect of bedding plane direction on acoustic emission characteristics of shale in Brazilian tests," *Rock and Soil Mechanics*, vol. 37, no. 6, pp. 1603–1612, 2016.

[19] J. Wang, L. Z. Xie, H. P. Xie et al., "Effect of layer orientation on acoustic emission characteristics of anisotropic shale in

Brazilian tests," *Journal of Natural Gas Science and Engineering*, vol. 36, pp. 1120–1129, 2016.

[20] J. M. He and L. O. Afolagboye, "Influence of layer orientation and interlayer bonding force on the mechanical behavior of shale under Brazilian test conditions," *Acta Mechanica Sinica*, vol. 34, no. 2, pp. 349–358, 2018.

[21] S. Q. Yang, P. F. Yin, and Y. H. Huang, "Experiment and discrete element modelling on strength, deformation and failure behaviour of shale under Brazilian compression," *Rock Mechanics and Rock Engineering*, vol. 52, no. 11, pp. 4339–4359, 2019.

[22] K. R. Liu and J. J. Sheng, "Experimental study of the effect of stress anisotropy on fracture propagation in eagle ford shale under water imbibition," *Engineering Geology*, vol. 249, pp. 13–22, 2019.

[23] J. Y. Teng, J. X. Tang, and C. Zhang, "Experimental study on tensile strength of layered water-bearing shale," *Rock and Soil Mechanics*, vol. 39, no. 4, pp. 1317–1326, 2018.

[24] H. C. She, Z. Q. Hu, Z. Qu, Y. Zhang, and H. Guo, "Determination of the hydration damage instability period in a shale borehole wall and its application to a fuling shale gas reservoir in China," *Geofluids*, vol. 2019, Article ID 3016563, 17 pages, 2019.

[25] Y. L. Lou, Z. H. Wu, W. J. B. Sun et al., "Study on failure models and fractal characteristics of shale under seepage-stress coupling," *Energy Science & Engineering*, vol. 8, no. 5, pp. 1634–1649, 2020.

[26] J. W. Carey, Z. Lei, E. Rougier, H. Mori, and H. Viswanathan, "Fracture-permeability behavior of shale," *Journal of Unconventional Oil and Gas Resources*, vol. 11, pp. 27–43, 2015.

[27] L. P. Frash, J. W. Carey, Z. Lei, E. Rougier, T. Lckes, and H. S. Viswanathan, "High-stress triaxial direct-shear fracturing of Utica shale and in situ X-ray microtomography with permeability measurement," *Journal of Geophysical Research: Solid Earth*, vol. 121, no. 7, pp. 5493–5508, 2016.

[28] F. Zhang, H. B. Liu, Y. F. Meng, S. Cui, and H. F. Ye, "Study on wellbore stability and failure regions of shaleconsidering the anisotropy of wellbore seepage," *Geofluids*, vol. 2021, Article ID 6694689, 13 pages, 2021.

[29] C. Liang, M. Chen, Y. Jin, and Y. H. Lu, "Wellbore stability model for shale gas reservoir considering the coupling of multi-weakness planes and porous flow," *Journal of Natural Gas Science and Engineering*, vol. 21, pp. 364–378, 2014.

[30] W. Z. Li, W. Li, F. Dai, X. Y. Xiao, and Q. B. Wen, "A new wellbore stability model for shale gas horizontal wells with effects of bedding planes and water content," *Chemistry and Technology of Fuels and Oils*, vol. 56, no. 5, pp. 783–791, 2020.

[31] Q. Zhang, X. Fan, P. Chen, T. Ma, and F. Zeng, "Geomechanical behaviors of shale after water absorption considering the combined effect of anisotropy and hydration," *Engineering Geology*, vol. 269, article 105547, 2020.

[32] S. Q. Yang, Y. H. Huang, Y. Y. Jiao, W. Zeng, and Q. L. Yu, "An experimental study on seepage behavior of sandstone material with different gas pressures," *Acta Mechanica Sinica*, vol. 31, no. 6, pp. 837–844, 2015.

[33] W. Xiao, D. Zhang, and X. Wang, "Experimental study on progressive failure process and permeability characteristics of red sandstone under seepage pressure," *Engineering Geology*, vol. 265, article 105406, 2020.

[34] J. Yu, W. Xu, C. Jia, R. Wang, and H. Wang, "Experimental measurement of permeability evolution in sandstone during hydrostatic compaction and triaxial deformation," *Bulletin of Engineering Geology and the Environment*, vol. 78, no. 7, pp. 5269–5280, 2019.

[35] P. S. Zhang, J. Q. Hou, C. Y. Zhao, and T. H. Li, "Experimental study on seepage characteristics of red sandstone with different confining pressures and different damage degrees," *Chinese Journal of Rock Mechanics and Engineering*, vol. 39, no. 12, pp. 2405–2415, 2020.

[36] P. S. Zhang, C. Y. Zhao, J. Q. Hou, T. H. Li, and X. Zhang, "Experimental study on seepage characteristics of deep sandstone under temperature-stress-seepage coupling conditions," *Chinese Journal of Rock Mechanics and Engineering*, vol. 39, no. 10, pp. 1957–1974, 2020.

[37] R. C. Liu, Q. Yin, H. Q. Yang, H. W. Jing, Y. J. Jiang, and L. Y. Yu, "Cyclic shear mechanical properties of 3D rough joint surfaces under constant normal stiffness (CNS) boundary conditions," *Chinese Journal of Rock Mechanics and Engineering*, vol. 40, no. 6, pp. 1092–1109, 2021.

[38] W. Guo, W. Shen, X. Li et al., "Study on mechanical characteristics and damage mechanism of the Longmaxi formation shale in southern Sichuan basin, China," *Energy Exploration & Exploitation*, vol. 38, no. 2, pp. 454–472, 2020.

[39] Y. Wang, Z. Q. Hou, and Y. Z. Hu, "In situ X-ray micro-CT for investigation of damage evolution in black shale under uniaxial compression," *Environmental Earth Sciences*, vol. 77, no. 20, pp. 1–12, 2018.

[40] E. Hoek and E. T. Brown, "Practical estimates of rock mass strength," *International Journal of Rock Mechanics and Mining Sciences*, vol. 34, no. 8, pp. 1165–1186, 1997.

[41] T. Ramamurthy and V. K. Arora, "Strength predictions for jointed rocks in confined and unconfined states," *International Journal of Rock Mechanics and Mining Sciences & Geomechanics Abstracts*, vol. 31, no. 1, pp. 9–22, 1994.